Supplementary Information

Wide-Linear Flexible Iontronic Pressure Sensor Enabled by Nanoparticle Interfacial Modulation and Synergistic Effect

Chenying He[1,2,3], Yuanao Zhang[1], Tao Zhou[1,2], Jian Chen[1,2*], Lei Wei[4], Chunlei Yang[1,2]and Ming Chen[1,2*]

[1]Shenzhen Institute of Advanced Technology, Chinese Academy of Sciences, Shenzhen 518055, People's Republic of China

[2]University of Chinese Academy of Sciences, Beijing 100049, People's Republic of China

[3]Department of Materials Science and Engineering, Southern University of Science and Technology, Shenzhen, 518055, People's Republic of China

[4]School of Electrical and Electronic Engineering, Nanyang Technological University, 50 Nanyang Avenue, 639798, Singapore

*Corresponding author: ming.chen2@siat.ac.cn. j.chen2@siat.ac.cn.

Keywords: Piezoelectric, ZnO, Synergistic Effect, high linearity , wide liner range.

Supplementary Note 1: Electrical characterization of TPU-IL-ZnO-SiO_2 films

An investigation of the electrical characteristics of the TPU-IL-ZnO-SiO_2 films under external pressure is key to clarifying the pressure-sensing mechanism of the ionic mechanoreceptor. Electrochemical impedance spectroscopy (EIS) is used to study ion-transport phenomena in polymer electrolytes and their interfaces (i.e., electrode-electrolyte interfaces). EIS measurements were performed at room temperature using an electrochemical analyzer PGSTAT302N (Metrohm Autolab) in a frequency range of 0.1 Hz to 100 kHz with a 20 mV AC perturbation. A coin cell assembly allowed us to perform EIS measurements of different TPU-IL-ZnO-SiO_2 films under different experimental conditions (with and without applied pressure).

For EIS measurements, TPU-IL-ZnO-SiO_2 films (~170 μm) were sandwiched between two stainless-steel discs (15 mm diameter used as electrodes) to achieve a capacitor device configuration. All impedance spectra were fitted using appropriate equivalent circuit models implemented in NOVA software (Metrohm Autolab) to

evaluate the bulk resistance (Rb) of the devices. The ionic conductivity was calculated from Rb values as follows: $\sigma=l/(Rb\times A)$, where σ is the ionic conductivity, l is the thickness of the polymer film, A is the area of the electrode, and Rb is the bulk resistance obtained from EIS Nyquist plots.

Supplementary Note 2: Test method of pressure sensing performance of TPU-IL-ZnO-SiO_2

The pressure-sensing performance of TPU-IL-ZnO-SiO_2 was evaluated using a capacitive device structure (ITO/TPU-IL-ZnO-SiO_2/ITO, film thickness ~170 μm, film area 1 cm^2) under a bias of 1 V at 1 kHz. We used indium tin oxide (ITO) glass as the model electrode to eliminate the influence of changes in the interfacial contact area between the TPU-IL-ZnO-SiO_2 thin film and deformable electrodes, thereby validating the concept of a confined ionic system with ultrasensitive pressure sensing capability over a wide pressure range.

Supplementary Note 3: CNN for human action recognition

As shown in **Figure S13**, the method is based on a multiscale kernel-based residual convolutional neural network (CNN)[15]. Firstly, the multiscale kernel algorithm is applied in the CNN architecture to ensure that different signal intensities are captured. The design of a multi-branch network ensures that the model can handle signals with varying intensities. Secondly, to enable the architecture to extract signal features from deep hierarchical representations, sufficient network depth is required. Therefore, residual learning is embedded in the multiscale CNN to avoid performance degradation and ensure effective feature extraction. Based on this design, the multi-time-scale convolutional network model has a clear structure and can effectively classify the input signals.

For human action recognition (HAR), the data are first fed into the initial convolutional layer for preprocessing, followed by max pooling. The processed features are then passed through the convolutional modules in batches, followed by average pooling, feature vector extraction, and concatenation for final classification.

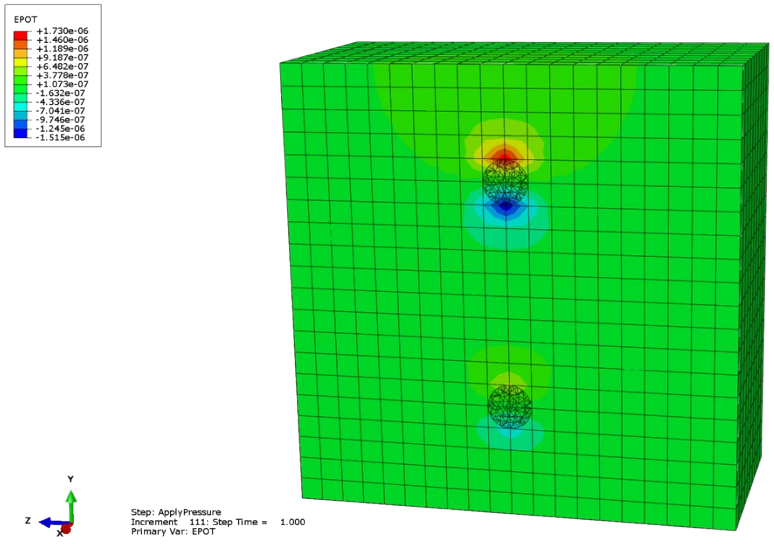

Supplementary Figure 1. Simulation Analysis of Piezoelectric Effect of ZnO in Ionogel under 100 kPa Pressure

Supplementary Figure 2. Thickness measurement of TPU-IL-ZnO-SiO_2 film.

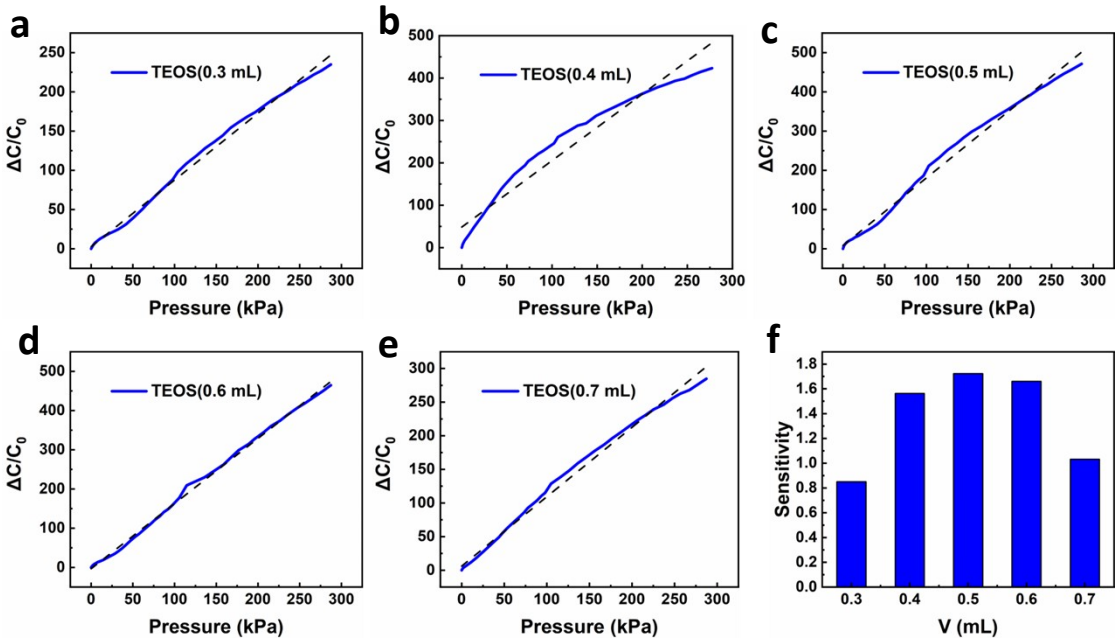

Supplementary Figure 3. Performance comparison of the capacitors with different TEOS contents. a-e) Pressure–capacitance curves of the devices with TEOS contents of 0.3, 0.4, 0.5, 0.6, and 0.7 mL, respectively. f) Sensitivity comparison of devices with different TEOS contents.

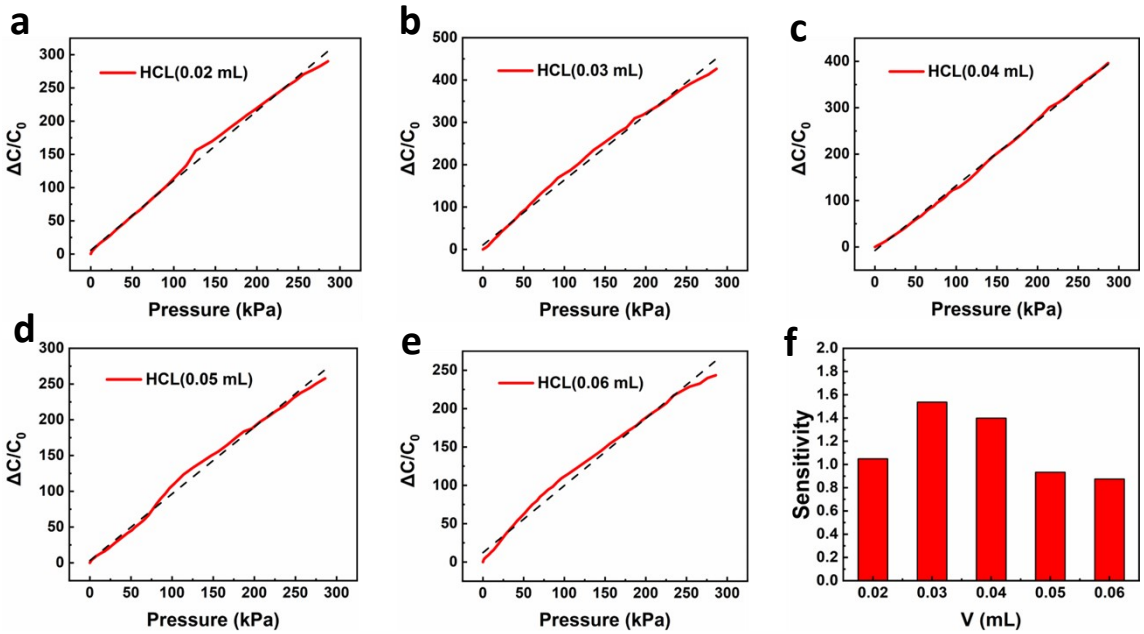

Supplementary Figure 4. Performance comparison of the sensor with different HCl contents. a–e) Pressure–capacitance curves of the devices with HCl contents of 0.02, 0.03, 0.04, 0.05, and 0.06 mL, respectively. f) Sensitivity comparison of devices with different HCl contents.

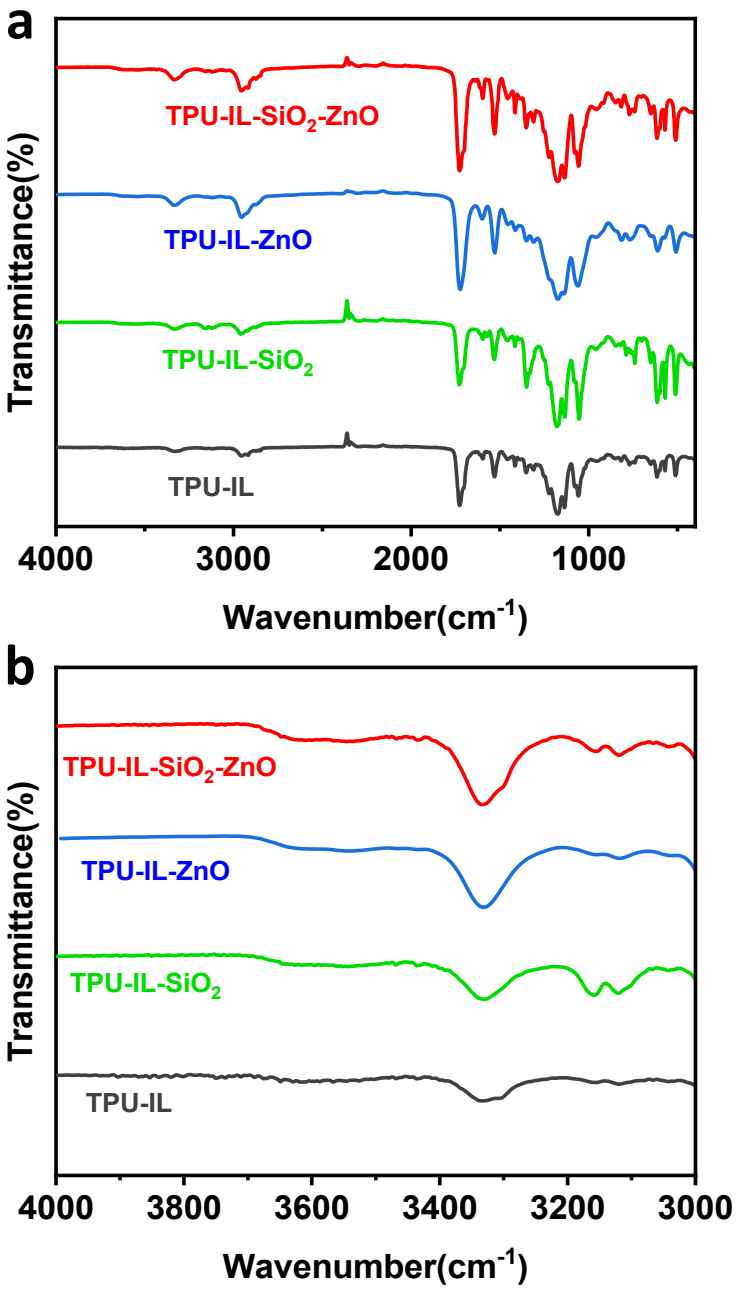

Supplementary Figure 5. FTIR spectra of TPU-IL, TPU-IL-SiO_2, TPU-IL-ZnO, and TPU-IL-SiO_2-ZnO films.

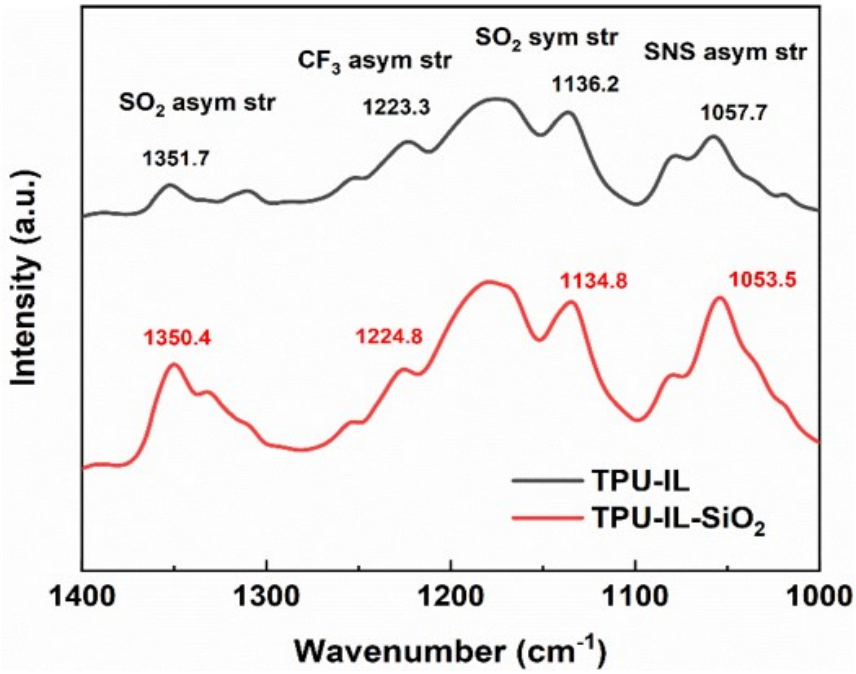

Supplementary Figure 6. Comparison of FTIR spectra between TPU-IL and TPU-IL-SiO_2 films.

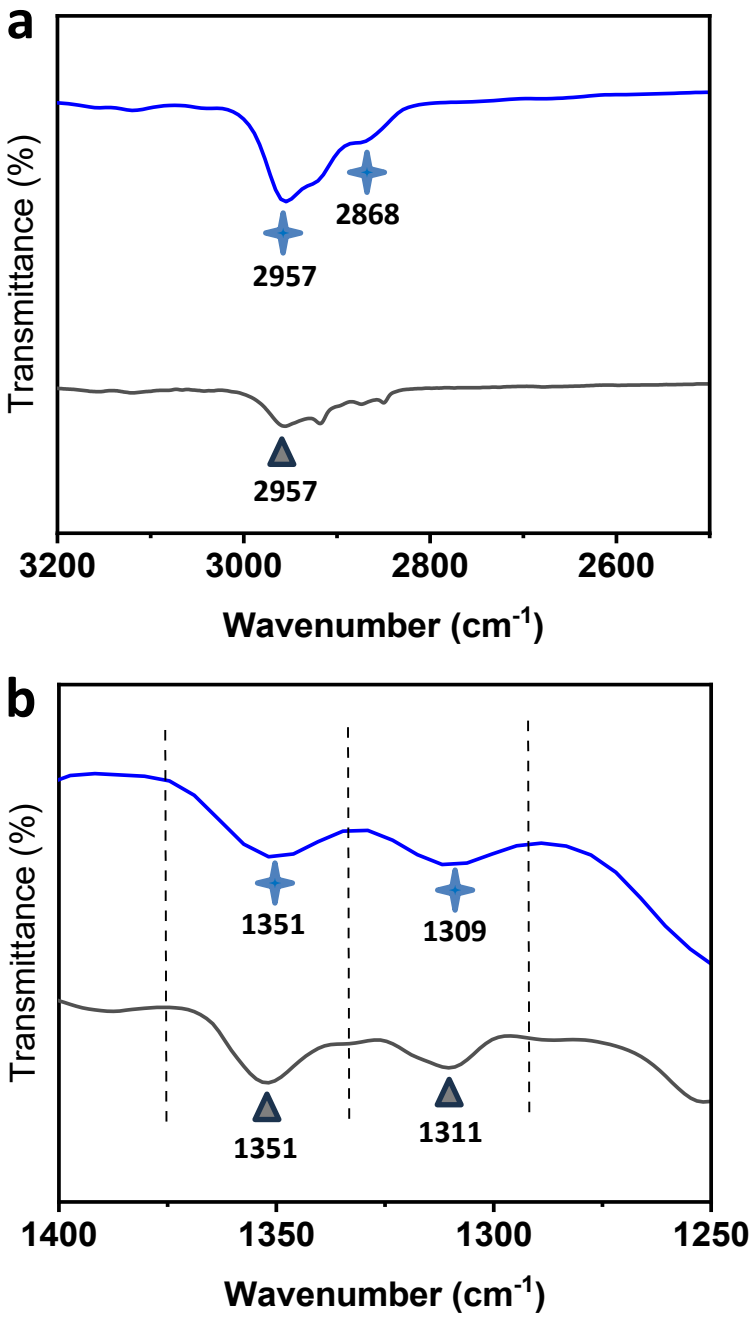

Supplementary Figure 7. Comparison of FTIR spectra between TPU-IL and TPU-IL-ZnO films.

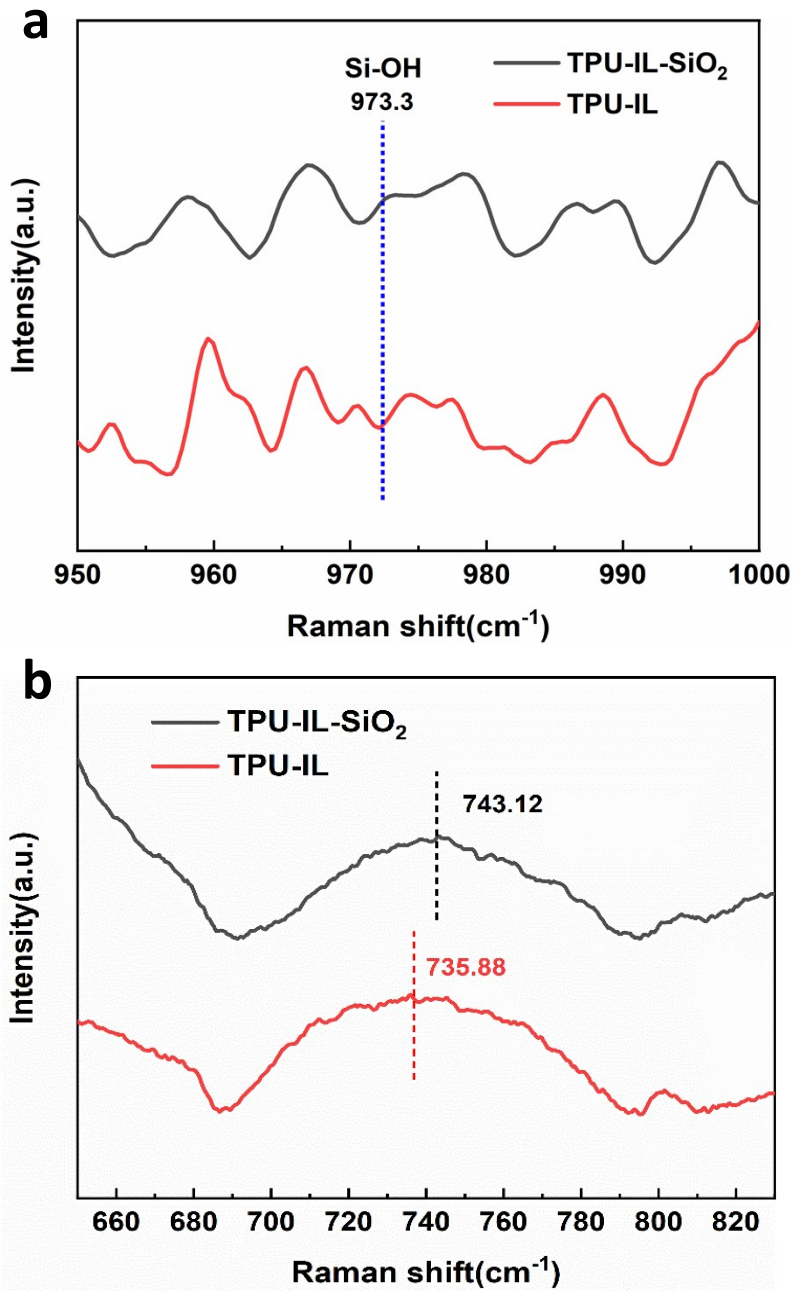

Supplementary Figure 8. Comparison of Raman spectra between TPU-IL and TPU-IL-SiO_2 films.

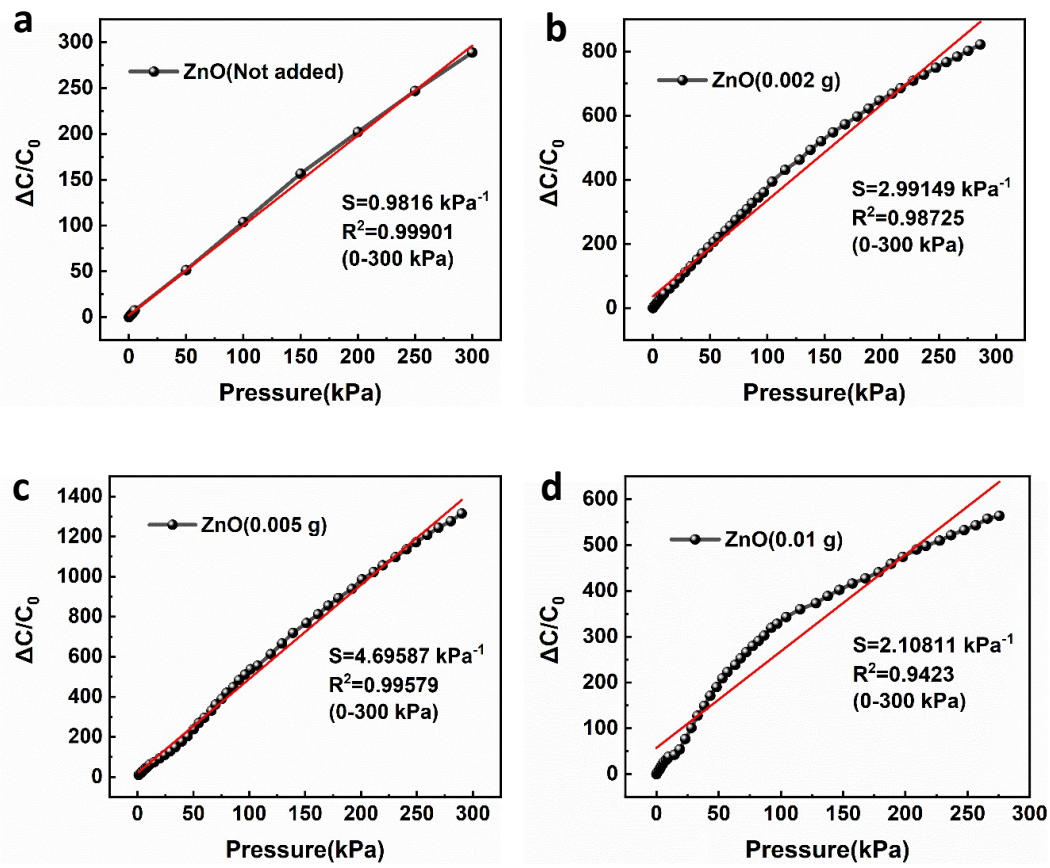

Supplementary Figure 9. Performance comparison of the sensors with different ZnO contents. (a) Pressure-capacitance curve and corresponding sensitivity of the device without ZnO NPs (TPU-IL-SiO_2); (b) Pressure-capacitance curve and corresponding sensitivity of the device with 0.002 g ZnO NPs; (c) Pressure-capacitance curve and corresponding sensitivity of the device with 0.005 g ZnO NPs; (d) Pressure-capacitance curve and corresponding sensitivity of the device with 0.01 g ZnO NPs.

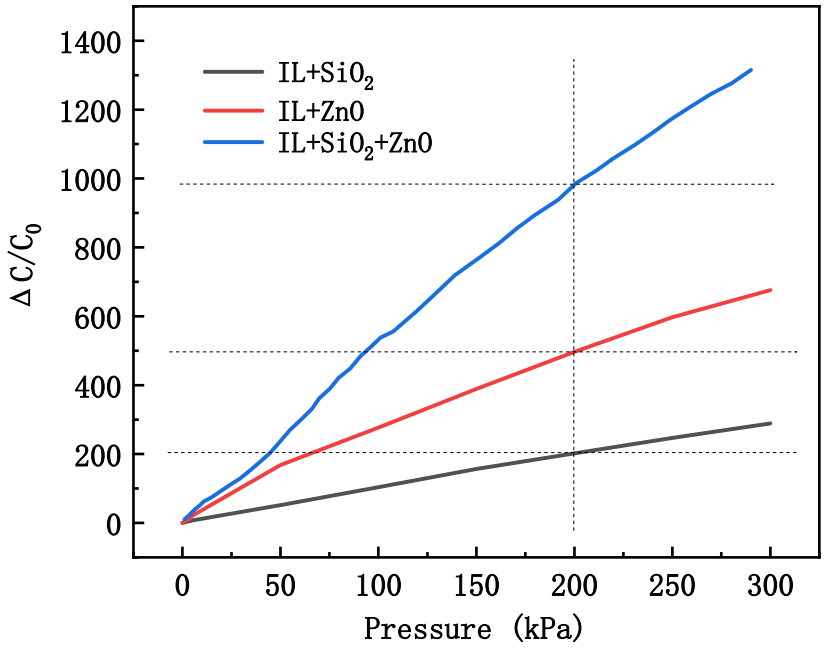

Supplementary Figure 10. Pressure-capacitance curves of the sensor devices with TPU-IL-SiO_2, TPU-IL-ZnO, and TPU-IL-SiO_2-ZnO layers.

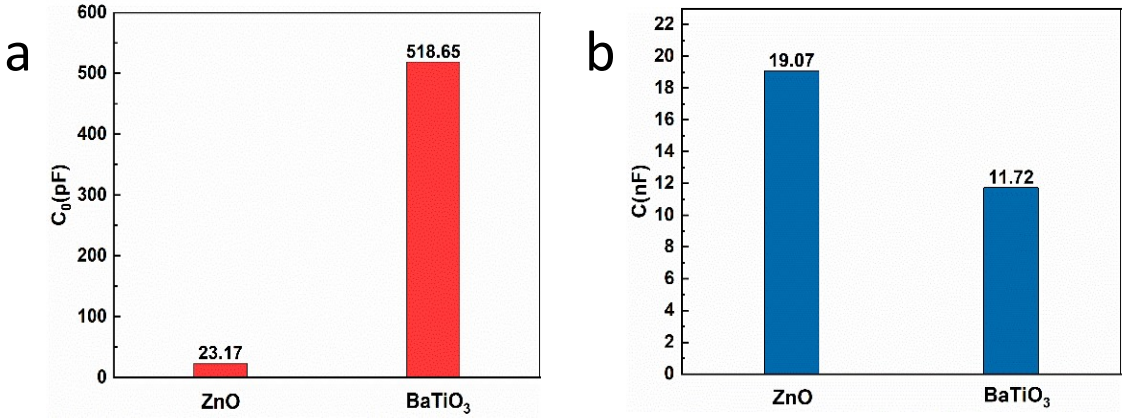

Supplementary Figure 11. (a) Initial capacitance of ionic films with different piezoelectric materials; (b) Capacitance of ionic films with different piezoelectric materials at 3 kPa.

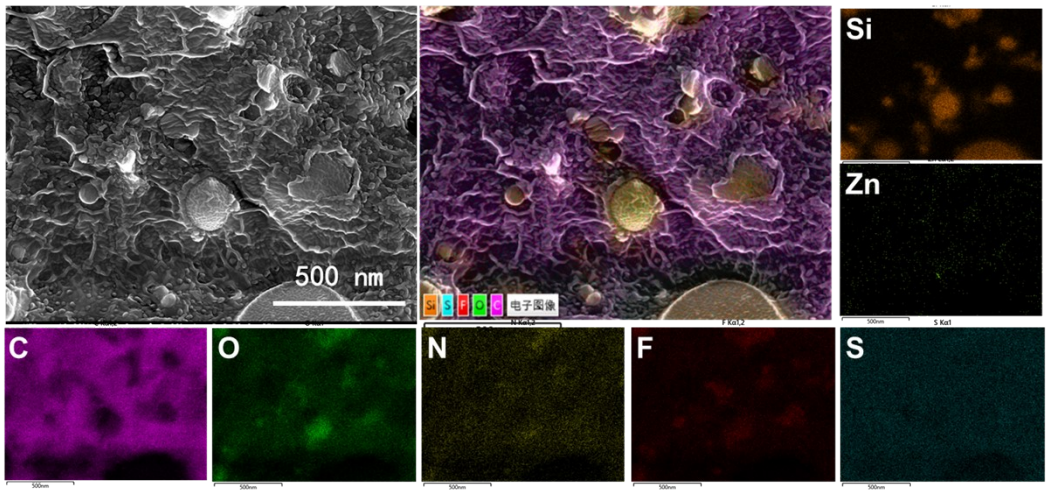

Supplementary Figure 12. FE-SEM image and EDS-elemental maps for C, O, F, N, S, Si and Zn of TPU-IL-ZnO-SiO_2 film.

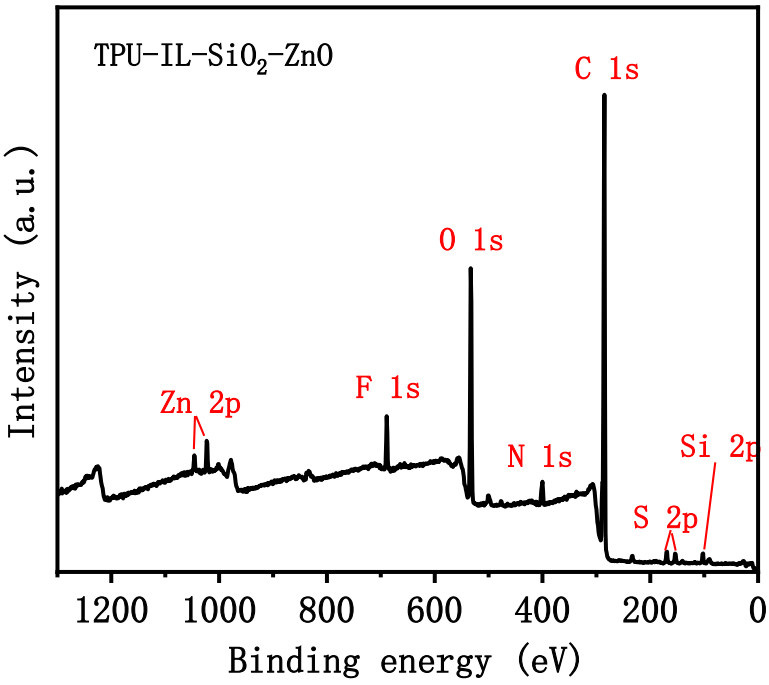

Supplementary Figure 13. XPS spectra of TPU-IL-SiO_2-ZnO films.

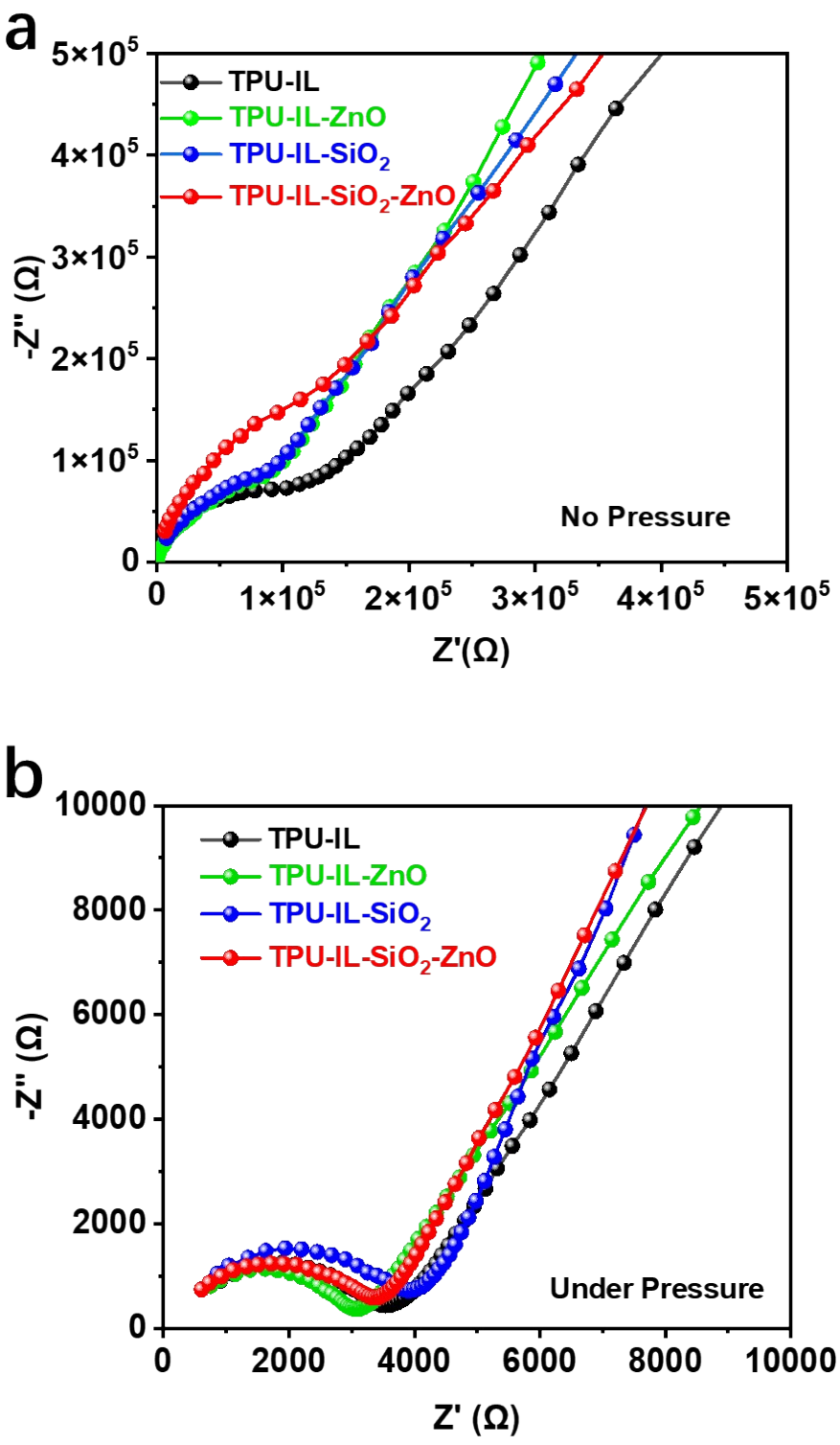

Supplementary Figure 14. (a) Impedance Nyquist plots of TPU-IL, TPU-IL-ZnO, TPU-IL-SiO_2, and TPU-IL-SiO_2-ZnO under no pressure. (b) Impedance Nyquist plots of TPU-IL, TPU-IL-ZnO, TPU-IL-SiO2, and TPU-IL-SiO2-ZnO under pressure.

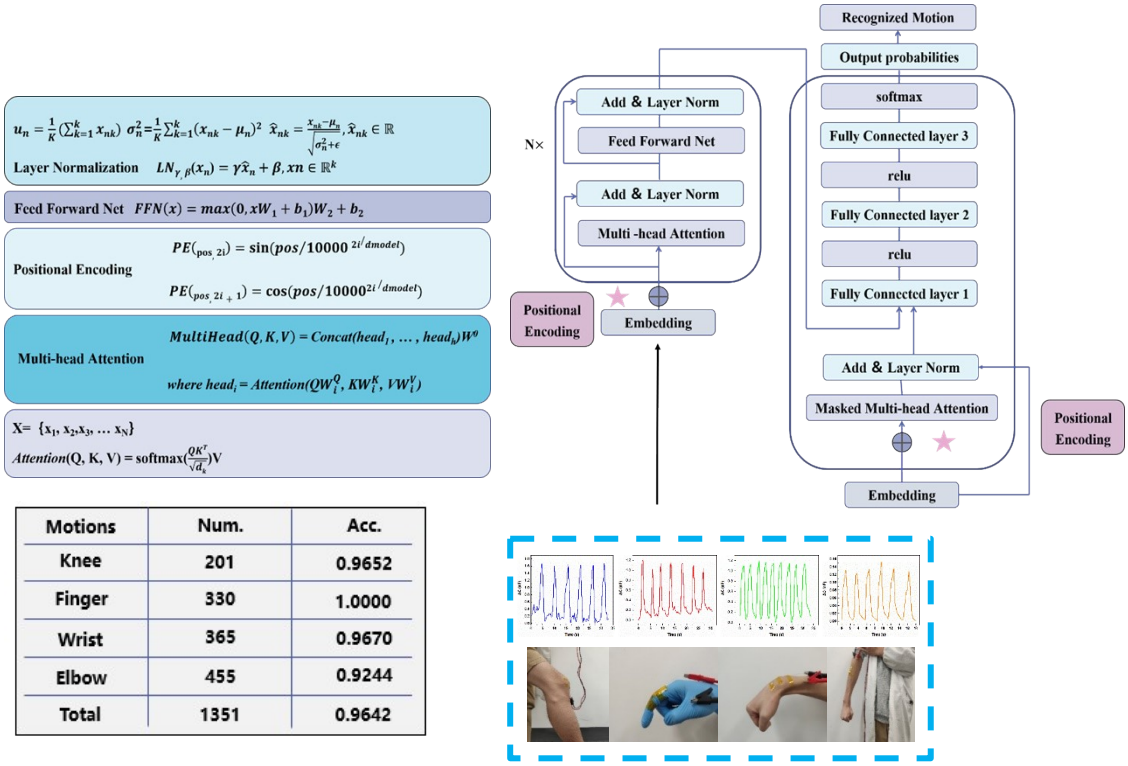

Motions	Num.	Acc.
Knee	201	0.9652
Finger	330	1.0000
Wrist	365	0.9670
Elbow	455	0.9244
Total	1351	0.9642

Supplementary Figure 15. Human action recognition based on multiscale kernel based residual convolutional neural network (CNN).

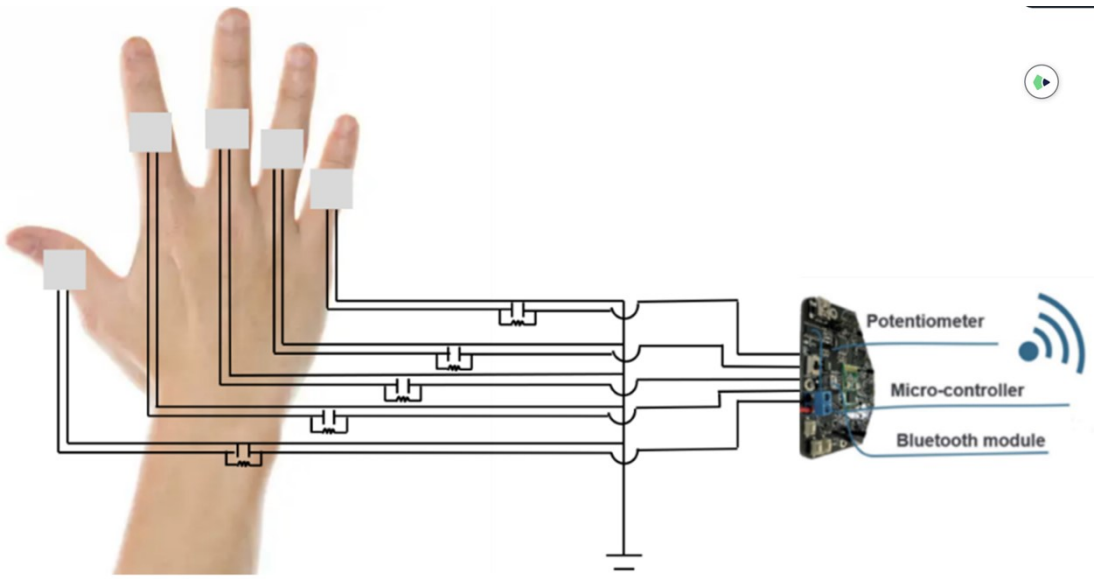

Supplementary Figure 16. Schematic of the smart glove, including multichannel sensor on the joints, resistance-capacitor filter, interconnectiong wiring, and wireless-control PCB layout.

Supplementary Table 1. Comparison of the pressure sensitivity and Linear Range of the pressure sensors obtained in this work with previously reported pressure sensors.

Device Type	Materials	Sensitivity (kPa^{-1})	Linear Range	References
Capacitive	PAM–NaCl/acrylic elastomer	0.01 (0–40 kPa)	0–40 kPa	1
Capacitive	Pt–coated polyurethane– based nanofibres	11.45 (~5 Pa)	0.005–1.5 kPa	2
Capacitive	PDMS/metal–coated hierarchical ZnO NW arrays	6.8 (< 0.3 kPa)	0.0006–0.3 kPa	3
Capacitive/ organic thinfilm pressure sensor	Microstructured PDMS dielectric	0.55 (< 2 kPa)	0–2 kPa	4
Piezoresistive	Polypyrrole/ITO–PET	56.0–133.1(< 0.03kPa)	10–30 Pa	5
Capacitive	CNT–Ecoflex/PorousEcoflex	0.601 (<5 kPa)	0–5 kPa	6
Organic thinfilm transistor type	PET–PDPP3T and CYTOPPI (semiconductor)/Al foil (suspended gate	192 (< 5 kPa)	0–5 kPa	7
Organic thinfilm transistor type	ITO–PET/MicrostructuredPDMS/	8.4 (< 2 kPa)	0–2 kPa	8
Piezoresistive	PVDF electrospun yarns of nanofibers coated with PEDOT	18.37 (~0.1 kPa)	0–0.1 kPa	9
Piezoresistive	Pt–PDMS/MWCNT–PDMS	15.1 (< 0.5 kPa)	0–0.5 kPa	10
Piezoresistive	Ultralight SparklingGraphene Block	229.8 (0–0.1 kPa)	0.02–0.1 kPa	11
Piezoresistive	Polystyrene ball@reduced graphene–oxide core–shell nanoparticles	50.9 (0.003–1 kPa)	0–1 kPa	12
Piezoresistive	ITO/IL–silica–TPU	48.1–33.18 (0–5 kPa)	0 –5 kPa	13
Capacitive	ITO/IL–HFMO–TPU	25.35	0-4 kPa	14
Capacitive	ITO/TPU-IL-SiO_2-	4.7	0-300 kPa	This work

Supplementary References

1. Sun, J-Y., Keplinger C., Whitesides G. M., & Suo, Z. Ionic skin. *Adv. Mater*. **26**, 7608–7614 (2014).
2. Ha, M. et al. Bioinspired interlocked and hierarchical design of ZnO nanowire arrays for static and dynamic pressure-sensitive electronic skins. *Adv. Funct. Mater*. **25**, 2841– 2849 (2015).
3. Kang, S. et al. Highly sensitive pressure sensor based on bioinspired porous structure for realtime tactile sensing. *Adv. Electron. Mater*. **2**, 1600356 (2016).
4. Mannsfeld, S. C. B. et al. Highly sensitive flexible pressure sensors with microstructured rubber dielectric layers. *Nature Mater*. **9**, 859–864 (2010).
5. Pan, L. et al. An ultra-sensitive resistive pressure sensor based on hollow-sphere microstructure induced elasticity in conducting polymer film. *Nat. Commun.* **5**, 3002 (2014).
6. Kwon, D. et al. Highly sensitive, flexible, and wearable pressure sensor based on a giant piezocapacitive effect of three-dimensional microporous elastomeric dielectric layer. *ACS Appl. Mater. Interfaces* **8**, 16922–16931 (2016).
7. Zang, Y. et al. Flexible suspended gate organic thin-film transistors for ultra-sensitive pressure detection. *Nat. Commun.* **6**, 6269, (2015).
8. Schwartz, G. et al. Flexible polymer transistors with high pressure sensitivity for application in electronic skin and health monitoring. *Nat. Commun.* **4**, 1859 (2013).
9. Zhou, Y. et al. Highly sensitive, self-powered and wearable electronic skin based on pressuresensitive nanofiber woven fabric sensor. *Sci Rep.* **7**, 12949 (2017).
10. Park, J. et al. Giant tunneling piezoresistance of composite elastomers with interlocked microdome arrays for ultrasensitive and multimodal electronic skins. *ACS Nano* **8**, 4689–4697 (2014).
11. Lv, L., Zhang, P., Xu, T. & Qu, L. Ultrasensitive pressure sensor based on an ultralight sparkling graphene bock. *ACS Appl. Mater. Interfaces* **9**, 22885–22892 (2017).
12. Ai, Y. et al. An ultrasensitive flexible pressure sensor for multimodal wearable electronic skins based on large-scale polystyrene ball@reduced graphene-oxide core–shell nanoparticles. *J. Mater. Chem. C.* **6**, 5514–5520 (2018).
13. Amoli, V., Kim, J.S., Jee, E. et al. A bioinspired hydrogen bond-triggered ultrasensitive ionic mechanoreceptor skin. *Nat. Commun.* **10**, 4019 (2019).
14. He, C., Wu, L., Gu, G. et al. An ionic assisted enhancement strategy enabled high performance flexible pressure–temperature dual sensor. Nano Letters **24**(23), 7040-7047(2024).
15. Liu, R.; Wang, F.; Yang, B. and Qin, S. J. Multiscale Kernel Based Residual Convolutional Neural Network for Motor Fault Diagnosis Under Nonstationary Conditions. *In IEEE Transactions on Industrial Informatics*. **16**(6), 3797-3806(2020).